Article

Cite This: Biomacromolecules 2019, 20, 2360−2371

pubs.acs.org/Biomac

Supramolecular Modification of a Sequence-Controlled Collagen-Mimicking Polymer

Sergio Spaans,[†] Peter-Paul K. H. Fransen,[†] Maaike J. G. Schotman,[†] Ruben van der Wulp,[†] René P. M. Lafleur,[†] Sebastiaan G. J. M. Kluijtmans,[‡] and Patricia Y. W. Dankers*[,†]

[†]Institute for Complex Molecular Systems, Eindhoven University of Technology, P.O. Box 513, 5600 MB Eindhoven, The Netherlands

[‡]Fujifilm Manufacturing Europe B.V., P.O. Box 90156, 5000 LJ Tilburg, The Netherlands

Supporting Information

ABSTRACT: Structurally and functionally well-defined recombinant proteins are an interesting class of sequence-controlled macromolecules to which different crosslinking chemistries can be applied to tune their biological properties. Herein, we take advantage of a 571-residue recombinant peptide based on human collagen type I (RCPhC1), which we functionalized with supramolecular 4-fold hydrogen bonding ureido-pyrimidinone (UPy) moieties. By grafting supramolecular UPy moieties onto the backbone of RCPhC1 (UPy-RCPhC1), increased control over the polymer structure, assembly, gelation, and mechanical properties was achieved. In addition, by increasing the degree of UPy functionalization on RCPhC1, cardiomyocyte progenitor cells were cultured on "soft" (∼26 kPa) versus "stiff" (∼68−190 kPa) UPy-RCPhC1 hydrogels. Interestingly, increased stress fiber formation, focal adhesions, and proliferation were observed on stiffer compared to softer substrates, owing to the formation of stronger cell−material interactions. In conclusion, a bioinspired hydrogel material was designed by a combination of two well-known natural components, i.e., a protein as sequence-controlled polymer and UPy units inspired on nucleobases.

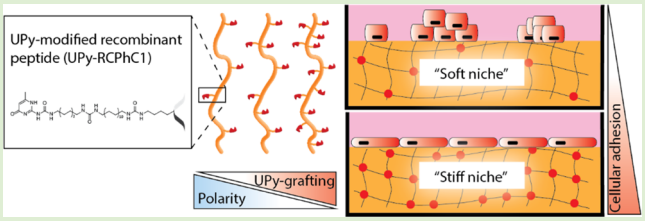

INTRODUCTION

The extracellular matrix (ECM) acts as a natural scaffold for cells and is important for the regulation and maintenance of cellular fate in terms of tissue development and pathology.[1−3] Many researchers have studied the influence of different ECM properties and the effect on cellular behavior for improved cell-based tissue regeneration.[4] Hydrogels are a class of biomaterials that resemble natural tissues with respect to their viscoelastic behavior. As such, hydrogels are commonly used as instructive microenvironments for cells.[5−7] Hydrogel-based biomaterials should display (i) optimal physical and mechanical properties that mimic the in vivo environment, (ii) sufficient adhesion sites to allow cells to adhere and migrate, and (iii) allow for cell-induced degradation.[8] In general, naturally derived hydrogels or materials, such as matrigel,[9] fibrin,[10] or collagen,[11] are used. These hydrogels contain high degrees of bioactive sites and therefore seem inexorable for the development of natural matrices.[12,13] However, these naturally based hydrogels have low controllability and often contain mixtures of different components and/or polymers with different lengths. Moreover, the synthesis of sequence-controlled synthetic polymers remains challenging in the field of polymer chemistry.[14]

It is proposed that recombinantly produced proteins are ideal candidates to develop biomaterials with full control of bioactive properties and polymer sequence, length and structure.[15−18] This is achieved using genetically modified organisms such as yeast or bacteria.[19] Additionally, protein-engineered biomaterials can be further functionalized to tune the biological and mechanical properties. Heilshorn et al., developed elastin-like polypeptide (ELP) hydrogels, in which the stiffness of the hydrogel network and arginine−glycine−aspartate (RGD) ligand density could be tuned independently.[20] This was done using tris(hydroxymethyl) phosphine (THP) to cross-link the poly(ethylene glycol) bis(amine) linker with specific amines located on the ELP. By changing the THP concentration, different storage moduli were obtained, ranging from 0.01 to 2.5 kPa. Encapsulated fibroblast cells showed more spread morphologies on the softer and compliant gels (∼1.3 kPa) compared to stiffer gels (∼2.5 kPa), as a result of the smaller hydrogel mesh size and increased crosslink density.[20] Another example of protein-engineered hydrogels is based on recombinant silk-based polypeptides.[18] Repeating units of glycine, alanine, and serine, in the backbone of silk-based polypeptides, induce the formation of β-sheets and consequently hydrogel networks can be formed.[21] With the high degree of control in molecular weight, polarity, and mechanical properties, recombinantly synthesized silk-based polypeptides are suitable to create biocompatible protein-engineered hydrogels.[22−24] These examples illustrate the

Received: March 11, 2019
Revised: April 29, 2019
Published: May 3, 2019

DOI: 10.1021/acs.biomac.9b00353
Biomacromolecules 2019, 20, 2360−2371

Scheme 1. Synthetic Procedure for Grafting UPy Functionalities to the Backbone of RCPhC1[a]

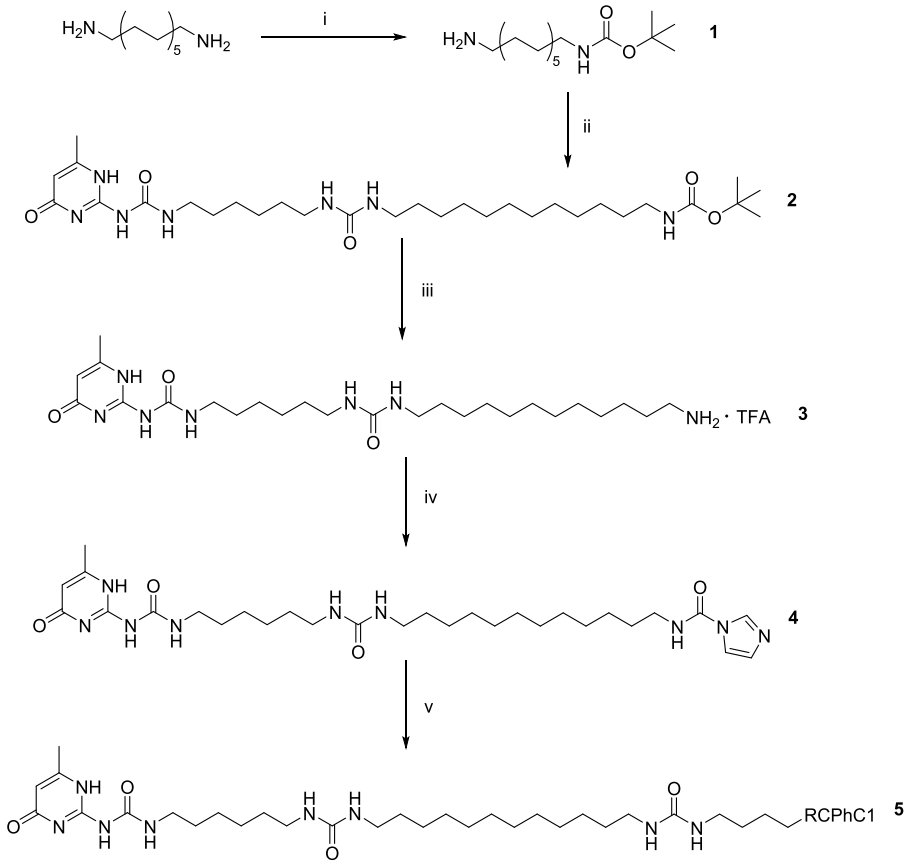

[a]Reaction conditions: (i) 0.33 equiv di-*tert*-butyl dicarbonate, chloroform ($CHCl_3$), 0 °C 1 h, rt, 24 h; (ii) 0.99 equiv ureido-pyrimidinone-hexyl-isocyanate, 1.7 equiv *N*,*N*-diisopropylethylamine, $CHCl_3$/methanol (MeOH) (3:1), rt, 4 h; (iii) $CHCl_3$/trifluoroacetic acid (TFA) (4:1), rt, 3 h; (iv) 1.0 equiv 1,1′-carbonyldiimidazole, 2 equiv *N*,*N*-diisopropylethylamine, dimethyl sulfoxide, rt, 1.5 h and; (v) different equivalents of RCPhC1 (see Table 1), dimethyl sulfoxide, 50 °C, argon, 24 h. *X* represents different amounts of grafted UPy groups determined with ^{1}H NMR.

benefit of recombinantly synthesized hydrogels for regenerative medicine purposes.

Recombinant peptides based on human collagen type I (RCPhC1), commercially known as Cellnest (FujiFilm Manufacturing Europe BV), are protein-engineered macromolecules with controlled lengths and specific amino acid sequences. Moreover, repeating amino acid sequences based on the integrin-binding peptide, RGD, have been engineered into the backbone of RCPhC1, to enhance cellular adhesion.[25] Another advantage of the application of this recombinant collagen as the polymer is due to its defined length, controlled sequence, and low immunologic risk.[26] RCPhC1 was previously used as a scaffold for the delivery of adipose-derived cells,[25] as a synthetic extracellular matrix for the development of bone tissue,[27,28] and as a delivery vehicle for bone-morphogenic protein-2.[29,30] Depending on the application or cell type to be cultured, the RCPhC1 sequence can be designed and adapted with different cross-links, e.g., methacrylates,[31] to create protein-engineered hydrogels.

In this study, we used RCPhC1 as the polymer backbone for the introduction of supramolecular 2-ureido-4[^{1}H]-pyrimidinone (UPy) hydrogen bonding units, to achieve control over hydrogel formation, mechanical properties, and cellular response. Supramolecular UPy moieties were previously used to modify different synthetic polydisperse polymers such as hydrophilic poly(ethylene glycol) or polyesters such as polycaprolactone and hydrophobic amorphous priplast polymers, which illustrates the versatility of UPy-based supramolecular biomaterials.[32−34] Compared to covalently cross-linked hydrogels, UPy-modified hydrogels allow for the possibility to tune the material properties, such as stiffness, degradability, and bioactivity. Here, the degree of UPy substitution onto the backbone of RCPhC1 was varied and the structure, molecular assembly, and gelation are studied and characterized. By increasing the amount of grafted UPy groups, it is hypothesized that the stiffness of the hydrogel is increased. The applicability of UPy-modified RCPhC1 hydrogels as the two-dimensional cell culture matrix is tested using human cardiac progenitor cells (CPCs).[35] These cells are ideal candidates for cardiac regeneration applications due to their self-renewal, ECM production capacity, and potential to differentiate into cardiomyocytes.[36−38] Finally, the relationship between molecular interactions and assembly versus the observed cellular response is discussed.

EXPERIMENTAL SECTION

Materials. Chemicals and reagents were purchased from commercial sources at the highest purity available and used without further purification. All solvents were purchased from Sigma-Aldrich unless stated otherwise. Cellnest, a recombinant peptide based on human collagen type I (RCPhC1), was a gift from Fujifilm

DOI: 10.1021/acs.biomac.9b00353
Biomacromolecules 2019, 20, 2360−2371

Table 1. Degree of Functionalization of the UPy-RCPhC1 Derivatives Based on ^{1}H NMR

UPy-RCPhC1 derivative	RCPhC1-NH_2/UPy-CDI molar ratio	yield (%)	integral at 5.7−5.8 ppm	integral at 0.8−1.0 ppm	theoretical molecular weight (kg/mol)
UPy-RCPhC1-2	1:0.25	85.6	2.0	264	52.2
UPy-RCPhC1-5	1:0.5	90.4	5.2	264	53.8
UPy-RCPhC1-8	1:1	99.3	8.3	264	55.4
UPy-RCPhC1-12	1:1	81.2	12.4	264	57.4
UPy-RCPhC1-16	1:1	77.4	16.1	264	59.5

Manufacturing Europe B.V. and was used without further purification (Figure S1). Phosphate buffered saline (PBS) tablets were purchased from Sigma-Aldrich (pH 7.2−7.6). Trypsin−ethylenediaminetetraacetic acid (EDTA) solution was purchased from Sigma (0.5 g/L porcine trypsin and 0.2 g/L EDTA in Hank's balanced salt solution with phenol red). All compound concentrations were determined by weight.

Methods. *Analytical Techniques and Equipment.* Reverse-phase high-performance liquid chromatography−mass spectrometry (RP-HPLC−MS) was performed with a Thermo scientific LCQ fleet spectrometer. Proton nuclear magnetic resonance (^{1}H NMR) spectra were recorded on a 400 MHz NMR (Varian Mercury Vx or Varian 400MR) operating at 400 MHz to determine the degree of functionalization. Proton chemical shifts are reported in ppm downfield from tetramethylsilane using the resonance of the deuterated solvent as the internal standard. Samples for NMR were prepared in D_2O/KOD with pH ≈ 11 at a concentration of 25 mg/mL. The purity of RCPhC1 and UPy-RCPhC1 derivatives was determined with Waters Xevo G2 Quadrupole Time-of-Flight liquid chromatography−mass spectrometry equipped with an Agilent Polaris C18A reverse-phase column (ID 2.0 mm, length 100 mm). Derivatives were dissolved in H_2O (0.5 mg/mL) and flowed (0.3 mL/min) over the column using a 15−75% water/acetonitrile gradient with 0.1% formic acid prior to analysis in the positive mode in the mass spectrometer. Dynamic light scattering (DLS) was measured on a Malvern Zetasizer Nano, model ZMV2000, at a measurement angle of 90°. Circular dichroism (CD) measurements and thermal unfolding studies were done on a JASCO J-815 spectrometer equipped with a JASCO MPTC-490S temperature control system. ζ-Potential measurements were performed on a Malvern instrument Zetasizer (model Nano ZSP). Zetasizer software was used to process and analyze the data. Nanoindentations were performed on a PIUMA nanoindenter (Optics II) using either a probe with a tip radius of 24 or 21.5 μm and a cantilever stiffness of 0.53 or 4.71 N/m, respectively. Calibration factors were determined by performing indentations on polystyrene surfaces. Rheology was performed on a TA Instruments Discovery Hybrid 3 shear rheometer with a 25 mm Sandblasted Peltier plate. To prevent water evaporation, an oil trap based on silicone oil (Rhodorsil) was used to seal the hydrogel. Fluorescence images were obtained using a Zeiss Axiovert 200M fluorescence microscope or a Leica TCS SP5X confocal laser scanning microscope. Fluorescence for the CyQuant assay was measured on a Synergy HTX multimode plate reader (BioTek).

Synthesis of UPy-RCPhC1. To synthesize UPy-RCPhC1 (**5**), a UPy synthon containing 1,1′-carbonyldiimidazole (**4**) was first synthesized and then coupled to pristine RCPhC1 (Scheme 1).

*Synthesis of 12-Amino-dodecyl-boc (**1**).* A flask was charged with 1,12-dodecadiamine (15 g, 75.0 mmol, 3 equiv) and dissolved in chloroform ($CHCl_3$) (300 mL). The stirring solution was cooled in an ice-bath to 0 °C and a solution of di-*tert*-butyl dicarbonate (5.45 g, 25.0 mmol, 1 equiv) in $CHCl_3$ (50 mL) was added dropwise. After the reaction mixture was stirred for 24 h, the solvents were removed by rotary evaporation to yield a transparent oil. The oil was concentrated under vacuum for 1 h to form a white solid. The solid was dissolved in ethyl acetate (EtOAc) (400 mL) and washed with half-saturated brine (3 mL × 100 mL). Purification was performed by column chromatography (flash silica) with methanol (MeOH)−triethylamine (Et_3N) (10%)/dichloromethane (CH_2Cl_2) (10:90) affording 3.46 g (11.5 mmol, 46%) of **1** as a white solid. ^{1}H NMR ($CDCl_3$) δ (ppm): 4.53 (s, 1H), 3.09 (dd, 2H), 2.68 (t, 2H), 1.58 (s, 3H), 1.44 (s, 13H), 1.26 (s, 16H) (Figure S2). LC−MS electrospray ionization (ESI) *m*/*z* calcd ($C_{17}H_{36}N_2O_2$) 300.28; found 301.25 [M + H]$^+$.

*Synthesis of 12-(Ureido-pyrimidinone-hexyl-urea)-1-dodecyl-boc (**2**).* A round bottom flask was charged with ureido-pyrimidinone-hexyl-isocyanate (499 mg, 1.70 mmol, 1 equiv), monoprotected amine **1** (514 mg, 1.71 mmol, 1.01 equiv) and dissolved in $CHCl_3$ (30 mL) and MeOH (10 mL). *N*,*N*-Diisopropylethylamine (0.5 mL, 2.91 mmol, 1.7 equiv) was added to the stirring solution. After 4 h of stirring, the reaction mixture was purified on a short plug of silica eluting with $CHCl_3$/MeOH (1:1) to remove excess of amine **1**. The solvents were removed by rotary evaporation and concentrated under vacuum to yield 1.01 g (1.69 mmol, 99%) of **2** as a white waxy solid. ^{1}H NMR ($CDCl_3$/MeOD) δ (ppm): 5.86 (s, 1H), 3.28 (m, 2H), 3.11 (m, 6H), 2.26 (s, 3H), 1.59 (m, 2H), 1.44 (s, 15H), 1.36 (m, 4H), 1.25 (m, 18H) (Figure S3). LC−MS (ESI) *m*/*z* calcd ($C_{30}H_{55}N_7O_5$) 593.43; found 594.42 [M + H]$^+$.

*Synthesis of 12-(Ureido-pyrimidinone-hexyl-urea)-1-dodecyl-amine (**3**).* A round bottom flask was charged with compound **2** (355 mg, 0.60 mmol, 1 equiv), and dissolved in CH_2Cl_2 (16 mL). Trifluoroacetic acid (TFA) (4 mL) was added to the solution. After stirring the reaction mixture for 3 h, the solvents were evaporated by rotary evaporation and flushed with methanol to remove residual TFA to yield a light reddish oil. The oil was redissolved in $CHCl_3$/MeOH (3:1) and precipitated in Et_2O. The precipitate was concentrated under vacuum to yield 285 mg of **3** (0.47 mmol, 78%) as a TFA salt in the form of an off-white solid. ^{1}H NMR ($CDCL_3$/MeOD) δ (ppm): 5.91 (s, 1H), 3.24 (t, 2H), 3.10 (m, 4H), 2.89 (m, 2H), 2.27 (s, 3H), 1.64 (m, 2H), 1.57 (m, 2H), 1.46 (m, 4H), 1.36−1.26 (m, 20H) (Figure S4). LC−MS (ESI) *m*/*z* calcd ($C_{25}H_{47}N_7O_3$) 493.37; found 494.42 [M + H]$^+$.

*Synthesis of 1,1′-Carbonyldiimidazole-activated UPy Synthon (**4**) and UPy-RCPhC1 (**5**).* Preactivation was performed by dissolving compound **3** in dimethyl sulfoxide (2−5 mL), followed by the addition of *N*,*N*-diisopropylethylamine (2 equiv). Once dissolved, 1 equiv 1,1′-carbonyldiimidazole was added to the reaction mixture and allowed to react for 1.5 h. The formation of compound **4** was checked with RP-HPLC−MS before continuing with the next step (Figure S5). Recombinant peptide based on human collagen I (RCPhC1) (Figure S6) was dissolved in dimethyl sulfoxide and stirred under argon at 50 °C. Once dissolved, different equivalents of compound **4** was added to the reaction mixture to obtain different grafted UPy on the backbone of RCPhC1 (**5**) and stirred for 24 h at 50 °C. Next, the reaction mixture was precipitated in diethyl ether and centrifuged at 3500 rpm for 5 min. The obtained pellet was dissolved in 10 mL demi water/ethanol (1:1) solution. The reaction mixture was purified using a dialysis membrane (M_W cut-off = 3.5 kDa) in 800 mL demi water/ethanol (1:1) solution for 48 h and an additional 24 h in pure demi water. The purified solution was freeze-dried until a white material was obtained. The degree of substitution of compound **5** was determined with ^{1}H NMR (Table 1).

Hydrogel Formulation. 10 wt/vol % (100 mg/mL) hydrogels were created by first dissolving the UPy-RCPhC1 derivative in phosphate buffered saline (PBS) with pH = 12.7 (for 2, 5, and 8 UPy functionalities) or pH 12.9 (for 12 and 16 UPy functionalities) and was stirred at 50−70 °C until a homogenous solution was formed. Due to the different amounts of grafted UPy functionalities between

DOI: 10.1021/acs.biomac.9b00353
Biomacromolecules 2019, 20, 2360−2371

the different UPy-RCPhC1 polymers, different pH values were used to improve solubility. To readjust the pH and increase UPy−UPy association, D-glucono-δ-lactone (GDL) powder was mixed with the UPy-RCPhC1 solution. An amount of 10 mg/mL (for 2, 5, and 8 UPy functionalities) or 20 mg/mL (for 12 and 16 UPy functionalities) of GDL powder was added for each hydrogel. Due to the hydrolysis of GDL to gluconic acid, the pH slowly reduces to pH = 5−6 after 24 h and hydrogels are formed.

Dynamic Light Scattering. Samples for DLS measurements were prepared by dissolving 2 mg/mL of each compound in PBS and annealing for 1 h at 70 °C. The samples were filtered before measurement with a Whatman poly(vinylidene difluoride) filter, 0.45 μm. The temperature was set at 20 °C and decreased to 5 °C with steps of 5 °C, equilibrating for 500 s before measuring.

ζ-Potential. The samples were dissolved in (4-(2-hydroxyethyl)-1-piperazineethanesulfonic acid) (1 mM, pH = 7.6) at a concentration of 0.1 mg/mL and filtered with a 0.45 μm collagen filter. A DTS1070 cuvette was used for measuring the ζ-potential. The samples were measured in triplo, at room temperature, with a 30 s equilibration time. Measurement duration was automated and automatic attenuation and voltage selection were turned on.

Circular Dichroism. Samples for CD measurements were prepared by dissolving 0.5 mg/mL of the compounds in ultrapure water and stirring for approximately 30 min. The higher functionalized compounds (UPy-RCPhC1-12, UPy-RCPhC1-16) were annealed for 30 min at 50 °C. Measurements were performed with a scan speed of 100 nm/min, data pitch of 0.25 nm, a response time of 0.5 s, a bandwidth of 2, and a path length of 0.1 cm. The spectra were measured from 170 to 300 nm. The signal was processed with "Adjacent Averaging", 5 points of window. Experiments were conducted at a concentration of 0.5 mg/mL in a 0.1 cm Hellma quartz cell. For each measurement, the temperature was increased initially to 60 °C and decreased with steps of 1 °C/min to 5 °C. The molar residual ellipticity was determined using the following equation[39]

$$[\theta] = \frac{\theta \times m}{C \times l \times n_z}$$

where θ is the ellipticity in millidegrees, m is the molecular weight in g/mol, c is the concentration in mg/mL, l is the path length in cm, and n_z is the number of amino acids in the peptide. Graphs are shown from 180 to 280 nm, due to the higher noise ratio observed below 200 nm and due to the wavelength absorption of water.

Cryogenic Transmission Electron Microscopy. Cryogenic transmission electron microscopy was performed using samples with a concentration of 0.5 or 5 mg/mL. Vitrified films were prepared using a computer-controlled vitrification robot (FEI Vitrobot Mark III, FEI Company) at 22 °C, and at a relative humidity of 100%. In the preparation chamber of the "Vitrobot", 3 μL sample was applied on a Lacey film (LC200-CU, Electron Microscopy Sciences). These films were surface plasma treated just prior to use, with a Cressington 208 carbon coater operating at 5 mA for 40 s. Excess sample was removed by blotting using filter paper for 3 s at −3 mm, and the thin film thus formed was plunged (acceleration about 3 g) into liquid ethane just above its freezing point. Vitrified films were transferred into the vacuum of a CryoTITAN equipped with a field emission gun that was operated at 300 kV, a post-column Gatan energy filter, and a 2048 × 2048 Gatan CCD camera. Micrographs were taken at low dose conditions, starting at a magnification of 6500 times with a defocus setting of 40 μm, and at a magnification of 24 000 times with defocus settings of 10 and 15 μm. The sizes of the observed micelles were measured manually using Fiji software.

Nanoindentations. Nanoindentation tests were applied to measure the mechanical properties of UPy-RCPhC1 hydrogels, which is based on a probe that is in contact with the surface of the material and is pushed through. Depending on the load (P), spherical tip radius (R_i), displacement (h), and stiffness of the cantilever, the effective Young's modulus (E_{eff}) can be determined via the following formula considering the Hertzian contact model[40]

$$E_{eff} = \frac{P \times 3/4}{\sqrt{R_i} \times h_e^{3/2}}$$

where the effective Young's modulus is derived from a certain percentage of the elastic−plastic loading regime, displacement h_e, of the loading curve. Hydrogels with volumes of 50 μL were formed in the cap of a 200 μL Eppendorf tube, which was glued inside a small Petri dish. Before measuring the mechanical properties, the Petri dishes were filled with serum-free media (M199, Gibco) to cover the hydrogels. Indentations were performed using a cantilever with a stiffness of 0.53 N/m and a tip radius of 24 μm or a cantilever with a stiffness of 4.71 N/m and a tip radius of 21.5 μm for hydrogels based on UPy-RCPhC1-5/UPy-RCPhC1-8 and UPy-RCPhC1-12/UPy-RCPhC1-16, respectively. Calibrations were performed before measurements and indentation profiles were identical for each hydrogel. The effective Young's modulus (E_{eff}) was determined using the Hertzian contact model which is fitted through 20−60% of the loading curves using DataViewer (Piuma, OPTICS11).

Rheological Analysis. Hydrogels were prepared as stated previously. Following the addition of GDL, the gelation was followed at a constant shear rate of 1 rad/s, strain amplitude of 1%, and temperature of 25 °C for 1 h until complete gelation. Temperature sweeps were performed from 45 to 5 °C with increments of 4 °C and at each temperature step, hydrogels were soaked for 5 min to allow equilibration of temperature and rearrangement of molecules.

Cell Experiments. L9TB cardiomyocyte progenitor cells (CPCs) were immortalized by lentiviral transduction of hTert and BMI-1 (L9TB).[35] CPCs were cultured in SP++ growth medium containing M199 (Gibco), which uses a bicarbonate buffer system, and EGM-2 BulletKit (Lonza) in a 3:1 volume ratio, supplemented with 10% fetal bovine serum, 1% penicillin/streptomycin (Lonza), and 1% nonessential amino acids (Gibco) at physiological pH. CPCs were routinely cultured on 0.1% gelatin-coated PS, passaged at 80−90% confluency and seeded at a concentration of 3.1×10^4 cells/cm^2. Hydrogels were washed with SP++ before seeding cells to remove any excess of gluconic acid.

Immunofluorescence Staining. CPCs cultured on UPy-RCPhC1 hydrogels were first washed with PBS, fixated in 3.7% formaldehyde (Merck) for 10 min, washed twice with PBS, and permeabilized with 0.5% Triton X-100 (Merck) for 10 min. Non-specific binding of antibodies was minimized by incubating in 2% horse serum in PBS for 20 min. Cells were then incubated with primary antibodies in 10% horse serum in PBS for 2 h at 4 °C. Subsequently, the cells were first washed with PBS and incubated with a secondary antibody and phalloidin-FITC for 1 h in PBS followed by incubation with 4′,6-diamidino-2-phenylindole (0.4 μg/mL) in PBS for 5 min. Finally, the samples were washed and mounted on cover glasses with Mowiol (Sigma). Information regarding primary and secondary antibodies are listed in the Supporting Information (Table S1). The samples were imaged with a confocal laser scanning microscope (Leica TCS SP5X).

Cell Proliferation Assay. CPCs cultured on UPy-RCPhC1 hydrogels were first washed with PBS and the culture plate was frozen at −80 °C. A commercially available CyQuant Assay was used to measure the fluorescence of a dye that binds to nucleic acids. Based on a standard curve of known cell numbers (Figure S21), the fluorescence could be translated into cell numbers for each sample.

Statistical Analysis. Data are presented as mean ± standard deviation (SD). These data consisted of nanoindentations, cell numbers, and particle size measured with cryo-transmission electron microscopy (TEM). All statistical differences were determined using a nonparametric Kruskal−Wallis test with Dunn's post hoc test. Probabilities of $p < 0.05$ were considered as significantly different. All statistical analyses were performed using GraphPad Prism 5 Software (GraphPad Software, Inc.)

RESULTS AND DISCUSSION

Synthesis and Characterization of UPy-RCPhC1 Derivatives. A 1,1′-carbonyldiimidazole (CDI)-activated UPy synthon composed of a urea group and a 12-carbon

DOI: 10.1021/acs.biomac.9b00353
Biomacromolecules 2019, 20, 2360−2371

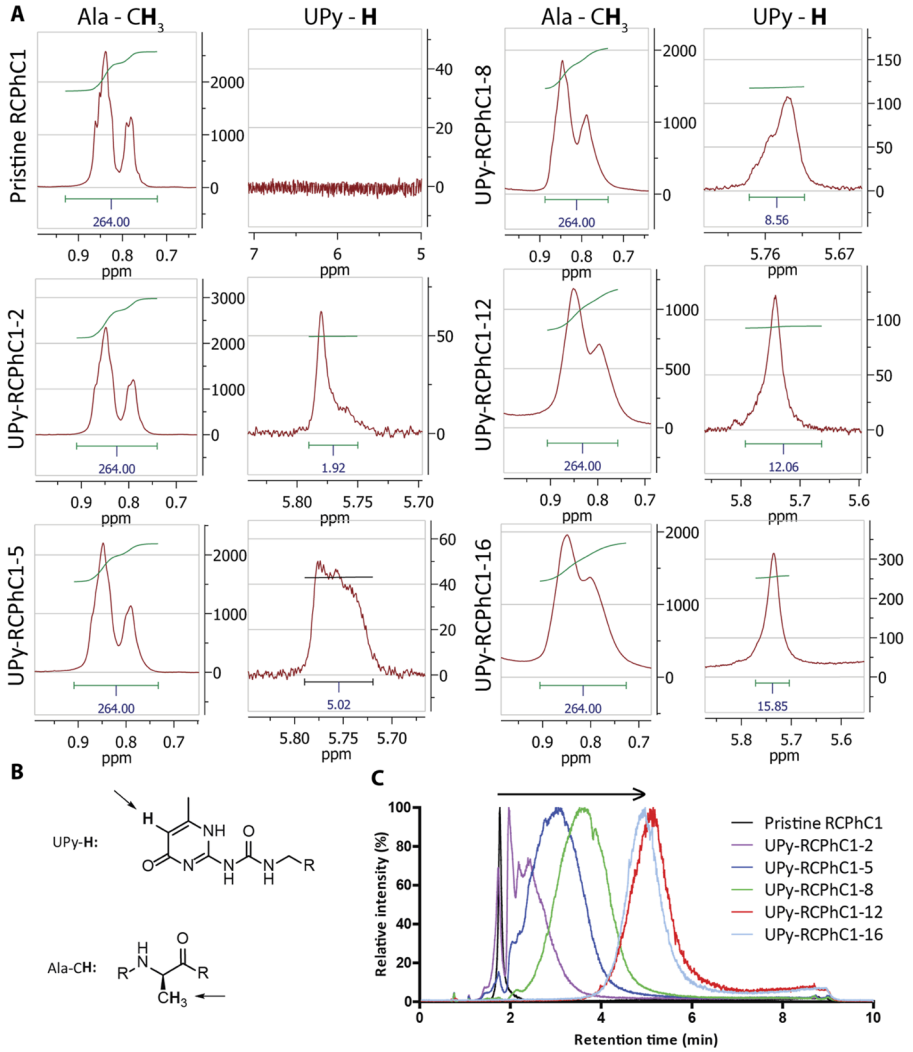

Figure 1. Characterization of supramolecular UPy-modified recombinant collagen peptide derivatives. (A) ^{1}H NMR graphs showing characteristic peaks of the protons on alanine residues (δ-shift = 0.7−0.9 ppm), which are used as the reference, and peaks of the alkylidene proton of the UPy groups (δ-shift = 5.7−5.8 ppm) for RCPhC1 and each UPy-RCPhC1 derivative. (B) Schematic representation of protons used to determine UPy conjugation, which is the alkylidene proton of the UPy group (UPy-**H**) and the protons on the methyl group on alanine groups (Ala-C**H**$_3$). (C) Chromatogram of UPy-RCPhC1 derivatives in H_2O (arrow indicates an increase in UPy grafting).

alkyl spacer **4** was designed and can be easily reacted with the RCPhC1 protein. The reaction involving CDI is fast and selective and thereby circumvents the need for any catalyst.[41] First, 1,12-dodecadiamine was protected with a boc-group yielding **1** (yield = 46%). Subsequently, **1** was reacted with UPy-hexyl-isocyanate, resulting in **2** (yield = 99%). Next, compound **2** was deprotected yielding amine-terminated UPy synthon **3** (yield = 78%). The CDI-activated UPy synthon **4** was synthesized by reacting amine-terminated UPy group **3** with CDI in the presence of a base. Finally, the CDI-activated UPy synthon **4** was reacted with nucleophilic amines on RCPhC1, which resulted in the formation of an additional urea group (Scheme 1). ^{1}H NMR was used to determine the amount of grafted UPy functionalities on RCPhC1 (Figure 1A). Due to the presence of a fixed number of 88 alanine residues on RCPhC1, the protons of methyl groups from the alanine side groups were used as a reference to determine the amount of grafted UPy groups on RCPhC1 (Figure 1B). Clearly, an increase in signal, corresponding to the UPy moiety, was observed upon increasing the feed ratio of CDI-activated UPy **4** (Figure 1A). However, some variations in the amount of grafted UPy functionalities were observed, which are likely due to the presence of impurities in the CDI-activated UPy synthon **4** (Table 1). With this approach, a library with different degrees of UPy substitutions, i.e., UPy-RCPhC1-2, UPy-RCPhC1-5, UPy-RCPhC1-8, UPy-RCPhC1-12, and UPy-RCPhC1-16, was achieved by varying the ratio of **4** to the amount of RCPhC1 (Figure S13). Based on RP-HPLC, broadening of the product is observed compared to pristine RCPhC1, which indicates increased polydispersity and multiple degrees of functionalization for UPy-RCPhC1 compounds (Figure 1C). Additionally, an increase in retention time is observed, which is likely due to the presence of an increased amount of hydrophobic alkyl spaced UPy functionalities (Figure 1C). Higher retention time was observed for UPy-RCPhC1-12 compared to UPy-RCPhC1-16, which could be due to the collapse of UPy-RCPhC1-16 in H_2O and a decrease in the interaction with the column of the chromatogram. The molecular weights of the UPy-RCPhC1 derivatives were determined using mass spectrometry for UPy-RCPhC1-2, -5, and -8 (Figures S8−S10). Due to the high degree of UPy conjugation and decrease of protonated amines, it was

DOI: 10.1021/acs.biomac.9b00353
Biomacromolecules 2019, 20, 2360−2371

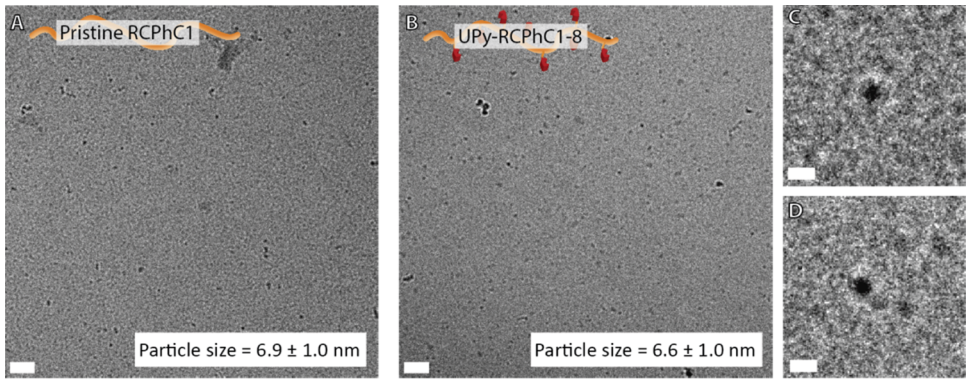

Figure 2. Cryogenic transmission electron microscopy images of diluted solutions of (A) 5 mg/mL RCPhC1 (left) and (B) 0.5 mg/mL UPy-RCPhC1-8 (right) in PBS (scale bar is equal to 50 nm). Particle sizes are indicated in the lower right part of the image and are shown as mean ± SD. Zoomed-in image of (C) RCPhC1 and (D) UPy-RCPhC1-8 (scale bar is equal to 10 nm).

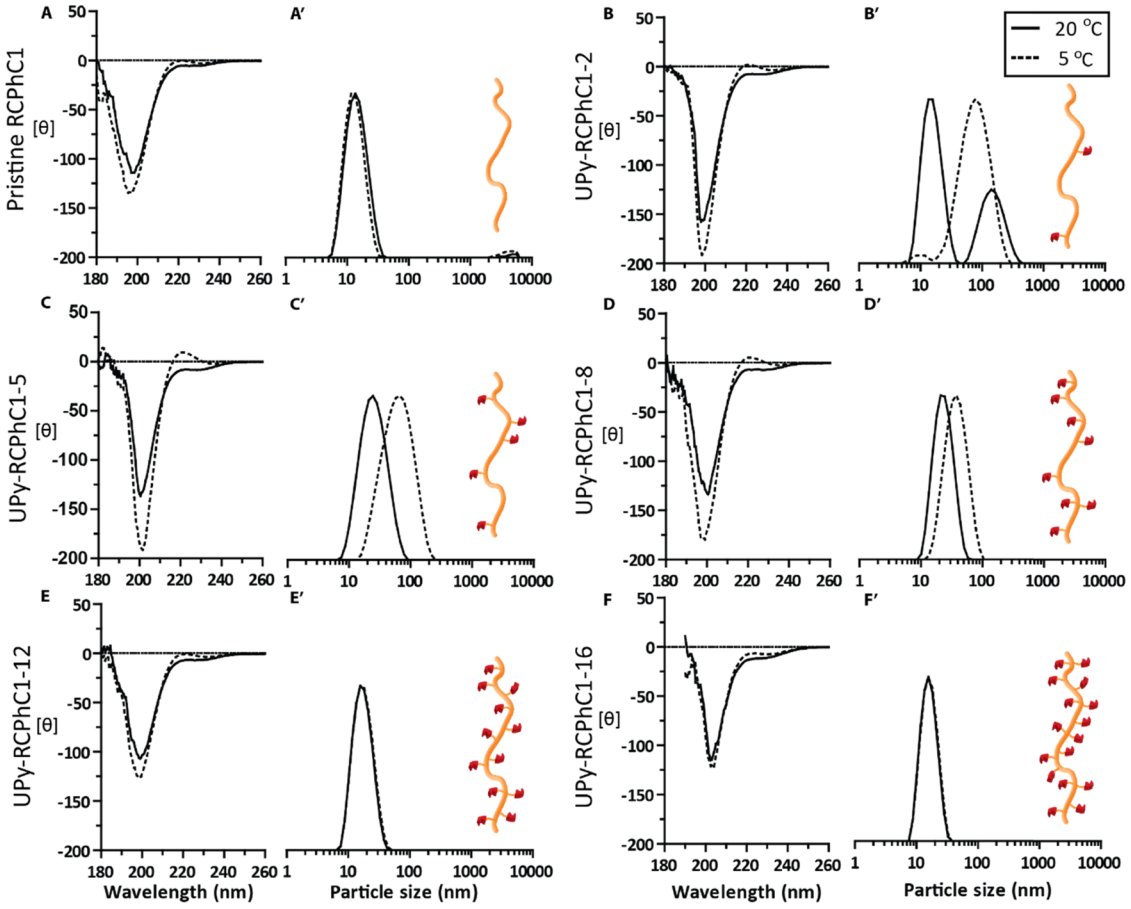

Figure 3. Structural analysis of RCPhC1 and UPy-RCPhC1 derivatives. (A−F) Circular dichroism graphs of RCPhC1 and UPy-RCPhC1 derivates measured at 20 °C (solid line) and 5 °C (dotted line) at a concentration of 0.5 mg/mL in ultrapure water. (A′−F′) Dynamic Light scattering measurements and normalized particle size distribution of RCPhC1 and UPy-RCPhC1 derivatives at 20 °C (solid line) and 5 °C (dotted line) at a concentration of 2 mg/mL in PBS.

impossible to determine the molecular weights of UPy-RCPhC1-12 and UPy-RCPhC1-16 (Figures S11 and S12). Nevertheless, a library containing different degrees of UPy substitutions was successfully synthesized (Figure S13). Additionally, due to the presence of grafted UPy functionalities, the supramolecular assembly can be studied based on the combination of hydrogen bonding and hydrophobic interactions (Figure S13).

Structure of RCPhC1 and UPy-RCPhC1 Derivatives. RCPhC1 is a sequence controlled, monodisperse polymer with a molecular weight of 51 kDa (Figure S7). In PBS solution, it assembles into particles with a size of 6.9 ± 1.0 nm, observed with Cryo-TEM (Figures 2A,C and S14). UPy-RCPhC1-8 shows a similar particle size of 6.6 ± 1.0 nm (Figures 2B,D and S14). These results show that the conjugation of at least 8 UPy groups to RCPhC1 does not have a large influence on the structural properties of pristine RCPhC1.

DOI: 10.1021/acs.biomac.9b00353
Biomacromolecules 2019, 20, 2360−2371

Table 2. Overview of the Mean ± SD of Triplicates of the Particle Size, Dispersity Index, and ζ-Potential of RCPhC1 and UPy-RCPhC1 Derivatives Measured with DLS at 20 and 5 °C

	size (nm)		dispersity index		
derivative	20 °C	5 °C	20 °C	5 °C	ζ-potential
RCPhC1	14.5 ± 1.1	13.2 ± 0.1	0.23 ± 0.05	0.17 ± 0.01	−6.1 ± 0.2
UPy-RCPhC1-2	21.3 ± 0.3	56.7 ± 5.6	0.43 ± 0.01	0.27 ± 0.02	−6.9 ± 0.1
UPy-RCPhC1-5	21.6 ± 0.1	50.9 ± 2.8	0.20 ± 0.01	0.21 ± 0.01	−9.4 ± 0.8
UPy-RCPhC1-8	21.6 ± 0.1	32.5 ± 1.4	0.10 ± 0.02	0.15 ± 0.01	−15.5 ± 0.7
UPy-RCPhC1-12	16.1 ± 0.1	16.1 ± 0.1	0.14 ± 0.01	0.13 ± 0.01	−29.0 ± 1.6
UPy-RCPhC1-16	15.2 ± 0.4	14.9 ± 0.1	0.12 ± 0.01	0.12 ± 0.01	−34.6 ± 2.0

It is known that RCPhC1 does not form organized triple helical structures typically seen for natural collagen type I.[42] However, due to the presence of proline residues in the amino acid sequence of RCPhC1, some secondary structures, categorized as "random coils", are formed similar to gelatin and can be detected with circular dichroism (CD).[39,43,44] Secondary structures formed by pristine RCPhC1 show a minimum at ∼195 nm and a maximum at ∼220 nm (Figure 3A). Upon cooling RCPhC1 to 5 °C, intermolecular interactions, based on hydrogen bonding, ionic and hydrophobic interactions, are stabilized and result in an increased CD effect, which is in agreement with other collagen-based peptides or proteins found in the literature (Figure 3A).[42] Moreover, after conjugating UPy groups to RCPhC1 a typical "random coil" structure and a small shift of the minima was observed (UPy-RCPhC1-2: ∼198 nm; UPy-RCPhC1-5: ∼202 nm; UPy-RCPhC1-8: ∼200 nm; UPy-RCPhC1-12: ∼198 nm; UPy-RCPhC1-16: ∼205 nm) (Figure 3B−F). This could simply be the result of small variations in the CD spectrum for the different UPy-RCPhC1 polymers, which indicate minimal differences in the secondary structure following covalent conjugation of UPy functionalities to residual amines. Interestingly, an increase of the CD effect was observed for all UPy-RCPhC1 derivatives upon cooling to 5 °C (Figure 3A−F). This effect illustrates that enhanced CD effects as a result of cooling and stabilization of intermolecular interactions are maintained following UPy conjugation. Moreover, functionalization of RCPhC1 with 2, 5, and 8 UPy groups resulted in an increase of the maxima at ∼220 nm, which was higher compared to pristine RCPhC1 (at 220 nm; RCPhC1: $[\theta]$ = −0.59; UPy-RCPhC1-2: $[\theta]$ = 1.27; UPy-RCPhC1-5: $[\theta]$ = 8.65; UPy-RCPhC1-8: $[\theta]$ = 5.14) (Figure 3A−D). It is proposed that a stabilization effect occurs as a result of UPy−UPy interactions, which enhances the CD effect and conceivably the secondary structure of RCPhC1.

Next, particle size distribution and information related to the aggregation of RCPhC1 and UPy-RCPhC1 derivatives were studied with dynamic light scattering (DLS) (Figure 3A′−F′ and Table 2). Pristine RCPhC1 had a particle size of 14.5 ± 1.1 nm, which is larger than the size observed with cryo-TEM (Figures 3A′ and 2A), an effect that is commonly observed and likely due to the hydration shell of the proteins.[45] No difference in particle size was observed upon cooling pristine RCPhC1 to 5 °C, which was not expected due to the increase in the CD effect, which was observed upon cooling as a result of stabilized intermolecular interactions. However, longer incubation time periods resulted in an increase in the particle size which indicates aggregation of RCPhC1 particles via weak intermolecular interactions (data not shown).

Functionalization of RCPhC1 with UPy groups resulted in a small increase in hydrodynamic particle size for UPy-RCPhC1-2 (21.3 ± 0.3 nm), UPy-RCPhC1-5 (21.6 ± 0.1 nm), and UPy-RCPhC1-8 (21.6 ± 0.1 nm) and similar particle size for UPy-RCPhC1-12 (16.1 ± 0.1 nm) and UPy-RCPhC1-16 (15.2 ± 0.4 nm) (Table 2). Similar to pristine RCPhC1, cooling of UPy-RCPhC1-12 and UPy-RCPhC1-16 to 5 °C did not change the particle size and dispersity index (Figure 3A′,E′,F′). For UPy-RCPhC1-2, 5, and 8, a clear increase in the hydrodynamic particle size and dispersity index is observed upon cooling the samples to 5 °C (Figure 3B′−D′). An increase of the dispersity index is the result of an increased dispersity of particle size within the sample, which is the result of aggregation and was only seen for intermediate UPy conjugations (2, 5, and 8). For UPy-RCPhC1-2, two distinct populations were observed at 20 °C (Figure 3B′). This is likely due to the presence of both grafted and unmodified RCPhC1, which results in different types of aggregation mechanisms and in the formation of larger and smaller particles. These results could be partially explained by the balance between intra- and intermolecular interactions and the polarity between the different UPy-RCPhC1 derivatives (Figure S16). By increasing the degree of functionalization of UPy groups, a decrease in polarity (Figure 1C) and a decrease of the ζ-potential of each UPy-RCPhC1 derivative were observed (Table 2). This is expected since polar and positively charged amine functional groups are replaced by hydrophobic UPy functionalities, which could influence the aggregation of UPy-RCPhC1 derivatives via their RCPhC1−RCPhC1 or UPy−UPy interactions. It is speculated that molecular packing and self-assembly via RCPhC1−RCPhC1 and/or UPy−UPy interactions are enhanced for the intermediate degree of functionalization (UPy-RCPhC1-2, 5, and 8) due to the presence of sufficient free amines that enhance solubility while allowing for intermolecular interactions with carboxyl groups between UPy-RCPhC1 molecules. Accordingly, higher degrees of functionalization (UPy-RCPhC1-12 and 16) resulted in a decrease in polarity and solubility, which results in more dense molecular packing.

It is speculated that for higher UPy conjugations, more stable intramolecular interactions are formed based on hydrogen bonding and hydrophobic interactions of the UPy moieties, which results in a decrease in electrostatic interactions of free amines and carboxyl groups between UPy-RCPhC1 molecules (Figure S16). This could explain the decrease in the formation of larger aggregates in dilute solutions (Figure 2E′,F′) of UPy-RCPhC1-12 and UPy-RCPhC1-16. Since the aggregation behavior of UPy-RCPhC1 derivatives is dictated via both RCPhC1−RCPhC1 and UPy−UPy interactions, it remains difficult to elucidate the true effect of different degrees of UPy functionalization. For this reason, the pH was first increased (pH > 12) to dissociate UPy−UPy interactions and consequently decreased to also

DOI: 10.1021/acs.biomac.9b00353
Biomacromolecules 2019, 20, 2360−2371

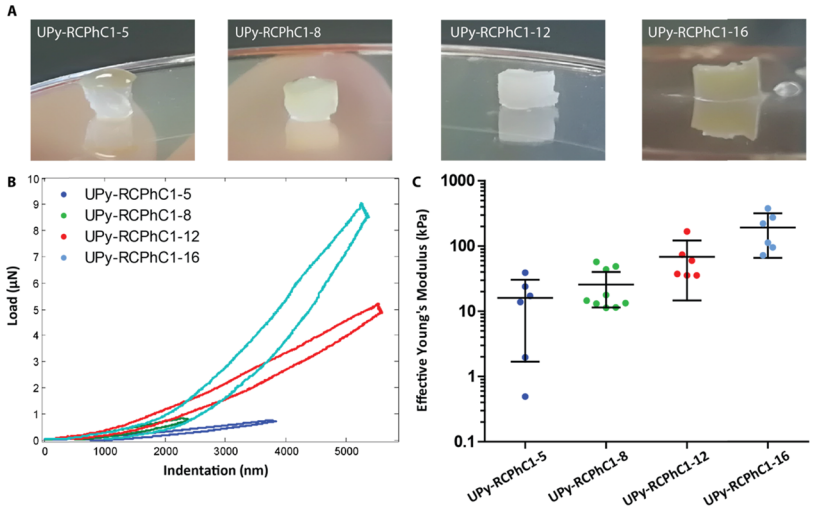

Figure 4. Mechanical characterization of UPy-RCPhC1 hydrogels measured with the Piuma Nanoindenter in serum-free cell culture medium (M199). (A) Images of UPy-RCPhC1 hydrogels showing a decrease in transparency as the amount of grafted UPy functionalities increases. (B) Representative load−displacement curves of each hydrogel, UPy-RCPhC1-5 (dark blue), UPy-RCPhC1-8 (green), UPy-RCPhC1-12 (red), and UPy-RCPhC1-16 (light blue). (C) Graph showing average values for the calculated effective Young's modulus (E_{eff}) for UPy-RCPhC1-5 (dark blue), UPy-RCPhC1-8 (green), UPy-RCPhC1-12 (red), and UPy-RCPhC1-16 (light blue) (10 wt/v %, 20 °C).

study the aggregation behavior at different temperatures. At elevated pH, RCPhC1 and UPy-RCPhC1 derivatives have a similar particle size; however, some subpopulations are observed for intermediate degrees of functionalization UPy-RCPhC1-2, -5, and -8 (Figure S15). Upon decreasing the temperature to 5 °C, no change in particle size is observed, which indicates a decrease in intermolecular interactions as a result of elevated pH. Upon lowering the pH, different particle size distribution and larger particle sizes were observed for RCPhC1 and all UPy-RCPhC1 derivatives. In addition, decreasing the temperature to 5 °C resulted in a wider distribution of the particle size (Figure S15). Moreover, for high degrees of UPy functionalizations, UPy-RCPhC1-12 and UPy-RCPhC1-16, larger aggregates formed after adjusting the pH. These results show the complexity of molecular aggregation as a result of changes in pH or temperature which is due to the presence of both RCPhC1−RCPhC1 and UPy−UPy interactions.

Hydrogel Formation and Mechanical Properties. The effect of increasing the degree of functionalization with UPy groups was also studied in concentrated solutions of UPy-RCPhC1 in PBS (100 mg/mL). The temperature was lowered to determine the liquid-gel cross-over of these solutions (Figure S17). In general, concentrated solutions of pristine RCPhC1 show a cross-over of the G' and G'' and gel formation at ∼10 °C. Interestingly, upon functionalization of RCPhC1 with on average 2 UPy groups and 5 UPy groups, an increase in cross-over temperature was observed, 14 and 16 °C, respectively (Figure S17). For UPy-RCPhC1-8, -12, and -16, a hydrogel was observed at all temperatures. These results clearly indicate the influence of UPy functionalities on the increase of cross-link formation and faster gelation.

Next, mechanical properties were measured using a nanoindenter, since loads (micronewton range) and scales (10−20 μm) are similar to what cells are able to sense. Interestingly, robust and stable hydrogels were formed through the modification of RCPhC1 with UPy functionalities (100 mg/mL, 20 °C) (Figure 4A). Hydrogels based on UPy-RCPhC1-5, 8, 12, and 16 remained intact at room temperature, however, an increase in opacity was observed as the degree of UPy functionalization increased (Figure 4A). This could be due to the presence of more UPy groups that cause the formation of larger aggregates within the hydrogel network, which resulted in decreased transparency. Interestingly, an increase in effective Young's modulus was observed upon increasing the degree of functionalization (Figure 4C). This is due to the presence of larger amounts of cross-links when more UPy groups are coupled to the backbone of RCPhC1. Indeed, the load−displacement curves recorded for each hydrogel show a local increase in the stiffness and maximum load (Figure 4B) and thereby confirm that the macroscopic properties we observe originate from our grafting strategy at the molecular scale. Here, it was chosen to study the response of mechanically sensitive cells, i.e., cardiac progenitor cells, on different UPy-RCPhC1 hydrogels as a culture platform. The stiffness of cardiac tissue typically ranges between 1−2 and 10−20 kPa from cardiac development up to mature cardiac tissue, respectively.[46−48] Additionally, following a myocardial infarction, a fibrotic scar is formed that typically displays a higher order of magnitude mechanical stiffness with Young's moduli of 35−70 kPa.[49] It was shown that embryonic cardiomyocytes respond differently on substrates with these mechanical rigidities.[49] For this reason, it is speculated that cardiac progenitor cells would also respond differently on "soft" UPy-RCPhC1-8 hydrogels (E_{eff} = 26 ± 19 kPa) compared to more rigid UPy-RCPhC1-12 and UPy-RCPhC1-16 hydrogels (E_{eff} = 68 ± 51 and 190 ± 118 kPa, respectively). Unfortunately, UPy-RCPhC1-2 and -5 did not form hydrogels at a concentration of 10 wt % at 37 °C.

CPC Behavior on UPy-RCPhC1 Hydrogels. Previous studies have determined the relationship between the mechanical stiffness of the environment and the biological response of cells.[50−52] Moreover, in the field of cardiac development and regeneration, the effect of the substrate stiffness on the adhesion, proliferation, and differentiation of cardiac progenitor cells have been thoroughly studied previously.[48,53] It was shown that matrix stiffness influences the genetic expression of cardiac progenitor cells (CPCs) via

DOI: 10.1021/acs.biomac.9b00353
Biomacromolecules 2019, 20, 2360−2371

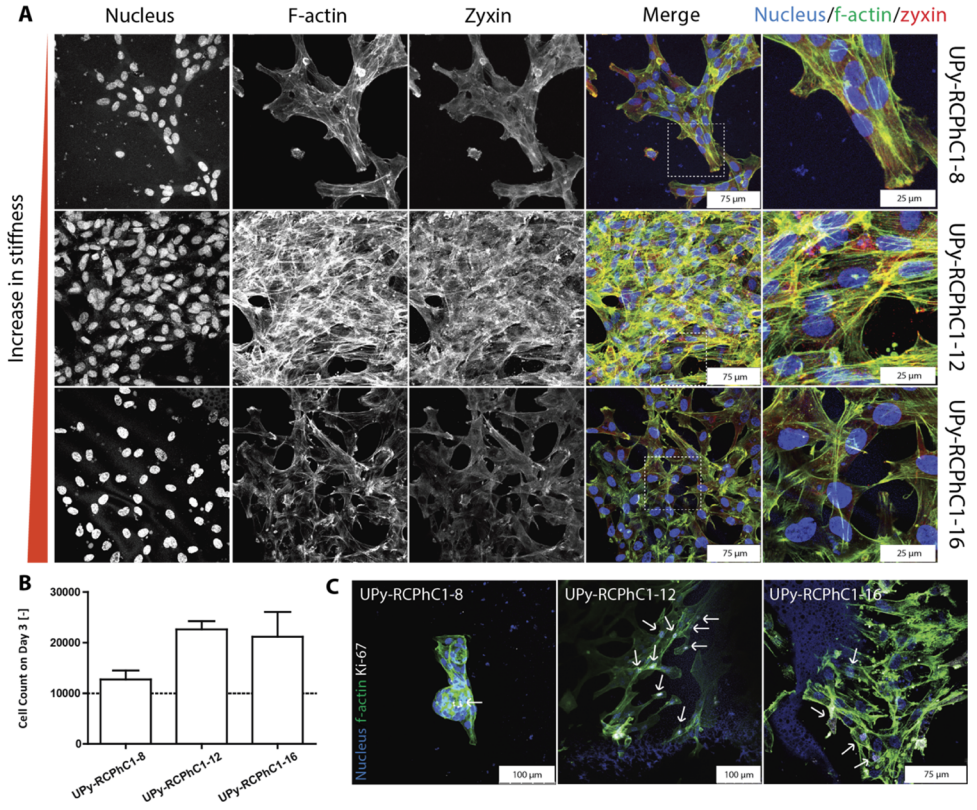

Figure 5. Cell adhesion and proliferation on UPy-RCPhC1 hydrogels. (A) Immunofluorescence images showing CPC distribution, f-actin stress fiber formation, and zyxin protein localization on (top-to-bottom) UPy-RCPhC1-8, UPy-RCPhC1-12, and UPy-RCPhC1-16. For each hydrogel, the individual channels, merged and zoomed images are shown from left-to-right, the nuclei (blue), f-actin stress fibers (green), zyxin (red), merged image and zoomed images (the dotted area is seen on the merged image). Scale bar is equal to 75 and 25 μm. (B) Graph showing the cell numbers after 3 days of culture on UPy-RCPhC1-8, UPy-RCPhC1-12, and UPy-RCPhC1-16. The dotted line represents seeded cells on day 0. (C) Immunofluorescence images showing ki-67 protein expression located at the nuclei after 3 days of culture on UPy-RCPhC1-8, UPy-RCPhC1-12, and UPy-RCPhC1-16. Ki-67 is shown in white, f-actin in green, nuclei in blue, and the scale bar is equal to 100 or 75 μm.

their mechanotransduction pathways.[36,54] Here, CPCs were cultured on top of UPy-RCPhC1-8, -12, and -16 hydrogels and both adhesion and proliferation were studied (Figure 5). The polymer concentration (10 wt %) and thereby the RGD concentration (each RCPhC1 molecule contains a fixed number of 12 RGD) were kept constant to study only the effect of substrate stiffness as a result of changing the UPy conjugation. Intriguingly, CPCs showed increased spreading and decreased clustering on stiffer UPy-RCPhC1-12 and -16 substrates compared to UPy-RCPhC1-8, which was coupled with an increase in stress fiber and zyxin formation after 1 day of culture (Figure 5A). Zyxin is a phosphoprotein which is located at the focal adhesions and thereby indicates a strong interaction between cells and their extracellular matrix.[55] Increased amounts of zyxin spots on UPy-RCPhC1 hydrogels could be due to increased stiffness, whereas on softer UPy-RCPhC1-8 surfaces cells favor cell clustering and cell−cell interactions due to the low mechanical rigidity (Figure 5A). Next, CPC proliferation was studied on UPy-RCPhC1-8, -12, and -16 after 3 days of culture (Figure 5B,C). For UPy-RCPhC1-8, CPCs showed low proliferation and cell numbers (Figure 5B) and low expression of proliferation marker ki-67 was observed (Figure 5C). For stiffer substrates based on UPy-RCPhC1-12 and -16, an increase in cell number (Figure 5B) and ki-67 expression was observed (Figure 5C).

These results indicate that the proliferation of CPCs is inhibited on softer substrates. These findings are in agreement with previous research; however, different rigidities and cell types were studied.[47,56] The mechanical stiffness of the substrate may also direct the cellular fate of CPCs or cardiac stem cells.[36] Therefore, we further studied the effect of stiffness of the different substrates on the behavior of CPCs. To this end, the intracellular Yes-associated protein (YAP) was stained and imaged (Figures S18 and S20). YAP is a downstream effector protein involved in the Hippo pathway that is a key player in sensing substrate stiffness and consequently driving cellular fate.[57−59] The mechanism is based on the translocation of YAP from the cytoplasm to the nucleus and results in downstream signaling related to proliferation and differentiation. Accordingly, immunofluorescence images show a minor increase of the YAP signal located at the nucleus compared to the cytoplasm on UPy-RCPhC1-12 hydrogels compared to UPy-RCPhC1-8 and UPy-RCPhC1-16 (Figure S18). However, due to the high degree of clustering, it remains inconclusive to relate the mechanical rigidity of the substrate with the YAP translocation, since it was shown that YAP mechanosensing is correlated to cell density regardless of the substrate rigidity.[60] Taken together, different degrees of CPC adhesion, proliferation, and YAP location was observed on the different UPy-RCPhC1 hydrogel substrates, which is speculated to be due the difference in crosslinking density and consequently the mechanical rigidity (Figure S19).

DOI: 10.1021/acs.biomac.9b00353
Biomacromolecules 2019, 20, 2360−2371

CONCLUSIONS

In this work, collagen-mimicking peptides were successfully modified with different degrees of supramolecular UPy groups. It was shown that the assembly and folding of UPy-RCPC1 were dependent on the degree of functionalization and resulted in an increased stability of intermolecular interactions based on UPy−UPy interactions. Additionally, increased control over hydrogel formation and mechanical properties compared to pristine RCPhC1 hydrogels was achieved. The applicability of this hydrogel was shown by a clear difference in focal adhesion formation and proliferation of CPCs, as a consequence of changing the mechanical rigidity. This work illustrates the versatility of modifying biomaterials with supramolecular UPy-based crosslinks for tissue engineering applications. In future work, UPy-RCPhC1 derivatives can be used as pH-sensitive injectable hydrogels (Figure S22) and as cellular carriers that act as synthetic extracellular matrices that used to enhance cellular-based tissue regeneration therapies.

ASSOCIATED CONTENT

Supporting Information

The Supporting Information is available free of charge on the ACS Publications website at DOI: 10.1021/acs.biomac.9b00353.

^{1}H NMR spectra, LC−MS spectra, mass spectra, schematic illustrations, cryo-TEM images, DLS, rheology, standard curves, and immunofluorescence images (PDF)

AUTHOR INFORMATION

Corresponding Author

*E-mail: p.y.w.dankers@tue.nl.

ORCID

Patricia Y. W. Dankers: 0000-0002-8997-181X

Author Contributions

This manuscript was written through contributions of all authors. All authors have given approval to the final version of the manuscript.

Notes

The authors declare no competing financial interest.

ACKNOWLEDGMENTS

We acknowledge the support from The Netherlands Cardiovascular Research Initiative (CVON2012-01 1_Valve; CVON2014-27 REMAIN), the Dutch Heart Foundation, Dutch Federation of University Medical Centers, The Netherlands Organization for Health Research and Development, and the Royal Netherlands Academy of Sciences. This work is part of the Gravitation research program Materials-Driven Regeneration with project number 024.003.013, which is partly financed by the Netherlands Organization for Scientific Research (NWO). The authors thank Fujifilm Manufacturing Europe in The Netherlands for providing pristine RCPhC1.

REFERENCES

(1) Jourdan-Lesaux, C.; Zhang, J.; Lindsey, M. L. Extracellular Matrix Roles during Cardiac Repair. *Life Sci.* **2010**, *87*, 391−400.

(2) Bouten, C. V. C.; Dankers, P. Y. W.; Driessen-Mol, A.; Pedron, S.; Brizard, A. M. A.; Baaijens, F. P. T. Substrates for Cardiovascular Tissue Engineering. *Adv. Drug Delivery Rev.* **2011**, *63*, 221−241.

(3) Gattazzo, F.; Urciuolo, A.; Bonaldo, P. Extracellular Matrix: A Dynamic Microenvironment for Stem Cell Niche. *Biochim. Biophys. Acta, Gen. Subj.* **2014**, *1840*, 2506−2519.

(4) Farhat, W.; Hasan, A.; Lucia, L.; Becquart, F.; Ayoub, A.; Kobeissy, F. Hydrogels for Advanced Stem Cell Therapies: A Biomimetic Materials Approach for Enhancing Natural Tissue Function. *IEEE Rev. Biomed. Eng.* **2019**, *12*, 333−351.

(5) Ooi, H. W.; Hafeez, S.; van Blitterswijk, C. A.; Moroni, L.; Baker, M. B. Hydrogels That Listen to Cells: A Review of Cell-Responsive Strategies in Biomaterial Design for Tissue Regeneration. *Mater. Horiz.* **2017**, *4*, 1020−1040.

(6) Tibbitt, M. W.; Anseth, K. S. Hydrogels as Extracellular Matrix Mimics for 3D Cell Culture. *Biotechnol. Bioeng.* **2009**, *103*, 655−663.

(7) Brown, T. E.; Anseth, K. S. Spatiotemporal Hydrogel Biomaterials for Regenerative Medicine. *Chem. Soc. Rev.* **2017**, *46*, 6532−6552.

(8) Goor, O. J. G. M.; Hendrikse, S. I. S.; Dankers, P. Y. W.; Meijer, E. W. From Supramolecular Polymers to Multi-Component Biomaterials. *Chem. Soc. Rev.* **2017**, *46*, 6621−6637.

(9) Hughes, C. S.; Postovit, L. M.; Lajoie, Ga. Matrigel: A Complex Protein Mixture Required for Optimal Growth of Cell Culture. *Proteomics* **2010**, *10*, 1886−1890.

(10) Ye, K. Y.; Sulllivan, K. E.; Black, L. D. Encapsulation of Cardiomyocytes in a Fibrin Hydrogel for Cardiac Tissue Engineering. *J. Visualized Exp.* **2011**, *55*, No. 3251.

(11) Chaudhuri, O.; Gu, L.; Klumpers, D.; Darnell, M.; Bencherif, S. A.; Weaver, J. C.; Huebsch, N.; Lee, H. P.; Lippens, E.; Duda, G. N.; et al. Hydrogels with Tunable Stress Relaxation Regulate Stem Cell Fate and Activity. *Nat. Mater.* **2016**, *15*, 326−334.

(12) Kleinman, H. K.; Martin, G. R. Matrigel: Basement Membrane Matrix with Biological Activity. *Semin. Cancer Biol.* **2005**, *15*, 378−386.

(13) Christman, K. L.; Fok, H. H.; Sievers, R. E.; Fang, Q.; Lee, R. J. Fibrin Glue Alone and Skeletal Myoblasts in a Fibrin Scaffold Preserve Cardiac Function after Myocardial Infarction. *Tissue Eng.* **2004**, *10*, 403−409.

(14) Ng, D. Y. W.; Wu, Y.; Kuan, S. L.; Wei, T. Programming Supramolecular Biohybrids as Precision Therapeutics. *Acc. Chem. Res.* **2014**, *47*, 3471−3480.

(15) Wang, H.; Zhu, D.; Paul, A.; Cai, L.; Enejder, A.; Yang, F.; Heilshorn, S. C. Covalently Adaptable Elastin-Like Protein-Hyaluronic Acid (ELP-HA) Hybrid Hydrogels with Secondary Thermoresponsive Crosslinking for Injectable Stem Cell Delivery. *Adv. Funct. Mater.* **2017**, *27*, No. 1605609.

(16) Wang, H.; Heilshorn, S. C. Adaptable Hydrogel Networks with Reversible Linkages for Tissue Engineering. *Adv. Mater.* **2015**, *27*, 3717−3736.

(17) DeForest, C. A.; Tirrell, D. A. A Photoreversible Protein-Patterning Approach for Guiding Stem Cell Fate in Three-Dimensional Gels. *Nat. Mater.* **2015**, *14*, 523−531.

(18) Jonker, A. M.; Löwik, D. W. P. M.; Van Hest, J. C. M. Peptide- and Protein-Based Hydrogels. *Chem. Mater.* **2012**, *24*, 759−773.

(19) Báez, J.; Olsen, D.; Polarek, J. W. Recombinant Microbial Systems for the Production of Human Collagen and Gelatin. *Appl. Microbiol. Biotechnol.* **2005**, *69*, 245−252.

(20) Wang, H.; Cai, L.; Paul, A.; Enejder, A.; Heilshorn, S. C. Hybrid Elastin-like Polypeptide-Polyethylene Glycol (ELP-PEG) Hydrogels with Improved Transparency and Independent Control of Matrix Mechanics and Cell Ligand Density. *Biomacromolecules* **2014**, *15*, 3421−3428.

(21) Werten, M. W. T.; Moers, A. P. H. A.; Vong, T. H.; Zuilhof, H.; van Hest, J. C. M.; de Wolf, F. A. Biosynthesis of an Amphiphilic Silk-like Polymer. *Biomacromolecules* **2008**, *9*, 1705−1711.

(22) Golinska, M. D.; Włodarczyk-Biegun, M. K.; Werten, M. W. T.; Stuart, M. A. C.; de Wolf, F. A.; de Vries, R. Dilute Self-Healing Hydrogels of Silk-Collagen-Like Block Copolypeptides at Neutral PH. *Biomacromolecules* **2014**, *15*, 699−706.

(23) Włodarczyk-Biegun, M. K.; Werten, M. W. T.; De Wolf, F. A.; Van Den Beucken, J. J. J. P.; Leeuwenburgh, S. C. G.; Kamperman,

DOI: 10.1021/acs.biomac.9b00353
Biomacromolecules 2019, 20, 2360−2371

M.; Cohen Stuart, M. A. Genetically Engineered Silk-Collagen-like Copolymer for Biomedical Applications: Production, Characterization and Evaluation of Cellular Response. *Acta Biomater.* **2014**, *10*, 3620−3629.
(24) Altman, G. H.; Diaz, F.; Jakuba, C.; Calabro, T.; Horan, R. L.; Chen, J.; Lu, H.; Richmond, J.; Kaplan, D. L. Silk-Based Biomaterials. *Biomaterials* **2003**, *24*, 401−416.
(25) Parvizi, M.; Plantinga, J. A.; Van Speuwel-Goossens, C. A. F. M.; Van Dongen, E. M. W. M.; Kluijtmans, S. G. J. M.; Harmsen, M. C. Development of Recombinant Collagen-Peptide-Based Vehicles for Delivery of Adipose-Derived Stromal Cells. *J. Biomed. Mater. Res., Part A* **2016**, *104*, 503−516.
(26) Tuin, A.; Kluijtmans, S. G.; Bouwstra, J. B.; Harmsen, M. C.; Van Luyn, M. J. A. Recombinant Gelatin Microspheres: Novel Formulations for Tissue Repair? *Tissue Eng., Part A* **2010**, *16*, 1811−1821.
(27) Ramírez-Rodríguez, G. B.; Montesi, M.; Panseri, S.; Sprio, S.; Tampieri, A.; Sandri, M. Biomineralized Recombinant Collagen-Based Scaffold Mimicking Native Bone Enhances Mesenchymal Stem Cell Interaction and Differentiation. *Tissue Eng., Part A* **2017**, *23*, 1423.
(28) Ramírez-Rodríguez, G. B.; Delgado-López, J. M.; Iafisco, M.; Montesi, M.; Sandri, M.; Sprio, S.; Tampieri, A. Biomimetic Mineralization of Recombinant Collagen Type I Derived Protein to Obtain Hybrid Matrices for Bone Regeneration. *J. Struct. Biol.* **2016**, *196*, 138−146.
(29) Mumcuoglu, D.; de Miguel, L.; Jekhmane, S.; Siverino, C.; Nickel, J.; Mueller, T. D.; van Leeuwen, J. P.; van Osch, G. J.; Kluijtmans, S. G. Collagen I Derived Recombinant Protein Microspheres as Novel Delivery Vehicles for Bone Morphogenetic Protein-2. *Mater. Sci. Eng., C* **2018**, *84*, 271−280.
(30) Mumcuoglu, D.; Fahmy-Garcia, S.; Ridwan, Y.; Nicke, J.; Farrell, E.; Kluijtmans, S.; van Osch, G. Injectable BMP-2 Delivery System Based on Collagen-Derived Microspheres and Alginate Induced Bone Formation in a Time- and Dose-Dependent Manner. *Eur. Cells Mater.* **2018**, *35*, 242−254.
(31) Sutter, M.; Siepmann, J.; Hennink, W. E.; Jiskoot, W. Recombinant Gelatin Hydrogels for the Sustained Release of Proteins. *J. Controlled Release* **2007**, *119*, 301−312.
(32) Mollet, B. B.; Spaans, S.; Fard, P. G.; Bax, N. A. M.; Bouten, C. V. C.; Dankers, P. Y. W. Mechanically Robust Electrospun Hydrogel Scaffolds Crosslinked via Supramolecular Interactions. *Macromol. Biosci.* **2017**, *17*, No. 1700053.
(33) Bastings, M. M. C.; Koudstaal, S.; Kieltyka, R. E.; Nakano, Y.; Pape, A. C. H.; Feyen, D. A. M.; van Slochteren, F. J.; Doevendans, P. A.; Sluijter, J. P. G.; Meijer, E. W.; et al. A Fast PH-Switchable and Self-Healing Supramolecular Hydrogel Carrier for Guided, Local Catheter Injection in the Infarcted Myocardium. *Adv. Healthcare Mater.* **2014**, *3*, 70−78.
(34) Spaans, S.; Fransen, P. P. K. H.; Ippel, B. D.; de Bont, D. F. A.; Keizer, H. M.; Bax, N. A. M.; Bouten, C. V. C.; Dankers, P. Y. W. Supramolecular Surface Functionalization via Catechols for the Improvement of Cell−Material Interactions. *Biomater. Sci.* **2017**, *5*, 1541−1548.
(35) Smits, A. M.; van Vliet, P.; Metz, C. H.; Korfage, T.; Sluijter, J. P.; Doevendans, P. A.; Goumans, M.-J. Human Cardiomyocyte Progenitor Cells Differentiate into Functional Mature Cardiomyocytes: An in Vitro Model for Studying Human Cardiac Physiology and Pathophysiology. *Nat. Protoc.* **2009**, *4*, 232−243.
(36) Mauretti, A.; Spaans, S.; Bax, N. A. M.; Sahlgren, C.; Bouten, C. V. C. Cardiac Progenitor Cells and the Interplay with Their Microenvironment. *Stem Cells Int.* **2017**, *2017*, 1−20.
(37) Bax, N. A. M.; van Marion, M. H.; Shah, B.; Goumans, M.-J.; Bouten, C. V. C.; van der Schaft, D. W. J. Matrix Production and Remodeling Capacity of Cardiomyocyte Progenitor Cells during in Vitro Differentiation. *J. Mol. Cell. Cardiol.* **2012**, *53*, 497−508.
(38) van Marion, M. H.; Bax, N. A. M.; van Turnhout, M. C.; Mauretti, A.; van der Schaft, D. W. J.; Goumans, M. J. T. H.; Bouten, C. V. C. Behavior of CMPCs in Unidirectional Constrained and Stress-Free 3D Hydrogels. *J. Mol. Cell. Cardiol.* **2015**, *87*, 79−91.
(39) O'Leary, L. E. R.; Fallas, J. A.; Bakota, E. L.; Kang, M. K.; Hartgerink, J. D. Multi-Hierarchical Self-Assembly of a Collagen Mimetic Peptide from Triple Helix to Nanofibre and Hydrogel. *Nat. Chem.* **2011**, *3*, 821−828.
(40) Fischer-Cripps, A. C. *Nanoindentation*, Mechanical Engineering Series; Springer: New York, NY, 2011.
(41) Vaidyanathan, R.; Kalthod, V. G.; Ngo, D. P.; Manley, J. M.; Lapekas, S. P. Amidations Using N,N′-Carbonyldiimidazole: Remarkable Rate Enhancement by Carbon Dioxide. *J. Org. Chem.* **2004**, *69*, 2565−2568.
(42) Pawelec, K. M.; Confalonieri, D.; Ehlicke, F.; van Boxtel, H. A.; Walles, H.; Kluijtmans, S. G. J. M. Osteogenesis and Mineralization of Mesenchymal Stem Cells in Collagen Type I-Based Recombinant Peptide Scaffolds. *J. Biomed. Mater. Res., Part A* **2017**, *105*, 1856−1866.
(43) Lopes, J. L. S.; Miles, A. J.; Whitmore, L.; Wallace, B. A. Distinct Circular Dichroism Spectroscopic Signatures of Polyproline II and Unordered Secondary Structures: Applications in Secondary Structure Analyses. *Protein Sci.* **2014**, *23*, 1765−1772.
(44) Greenfield, N. J. Using Circular Dichroism Spectra to Estimate Protein Secondary Structure. *Nat. Protoc.* **2006**, *1*, 2876−2890.
(45) Egelhaaf, S. U.; Wehrli, E.; Müller, M.; Adrian, M.; Schurtenberger, P. Determination of the Size Distribution of Lecithin Liposomes: A Comparative Study Using Freeze Fracture, Cryoelectron Microscopy and Dynamic Light Scattering. *J. Microsc.* **1996**, *184*, 214−228.
(46) Jacot, J. G.; Kita-Matsuo, H.; Wei, K. A.; Vincent Chen, H. S.; Omens, J. H.; Mercola, M.; McCulloch, A. D. Cardiac Myocyte Force Development during Differentiation and Maturation. *Ann. N. Y. Acad. Sci.* **2010**, *1188*, 121−127.
(47) Arshi, A.; Nakashima, Y.; Nakano, H.; Eaimkhong, S.; Evseenko, D.; Reed, J.; Stieg, A. Z.; Gimzewski, J. K.; Nakano, A. Rigid Microenvironments Promote Cardiac Differentiation of Mouse and Human Embryonic Stem Cells. *Sci. Technol. Adv. Mater.* **2013**, *14*, No. 025003.
(48) Hazeltine, L. B.; Badur, M. G.; Lian, X.; Das, A.; Han, W.; Palecek, S. P. Temporal Impact of Substrate Mechanics on Differentiation of Human Embryonic Stem Cells to Cardiomyocytes. *Acta Biomater.* **2014**, *10*, 604−612.
(49) Engler, A. J.; Carag-Krieger, C.; Johnson, C. P.; Raab, M.; Tang, H.-Y.; Speicher, D. W.; Sanger, J. W.; Sanger, J. M.; Discher, D. E. Embryonic Cardiomyocytes Beat Best on a Matrix with Heart-like Elasticity: Scar-like Rigidity Inhibits Beating. *J. Cell Sci.* **2008**, *121*, 3794−3802.
(50) Wen, J. H.; Vincent, L. G.; Fuhrmann, A.; Choi, Y. S.; Hribar, K. C.; Taylor-Weiner, H.; Chen, S.; Engler, A. J. Interplay of Matrix Stiffness and Protein Tethering in Stem Cell Differentiation. *Nat. Mater.* **2014**, *13*, 979−987.
(51) Trappmann, B.; Gautrot, J. E.; Connelly, J. T.; Strange, D. G. T.; Li, Y.; Oyen, M. L.; Cohen Stuart, M. A.; Boehm, H.; Li, B.; Vogel, V.; et al. Extracellular-Matrix Tethering Regulates Stem-Cell Fate. *Nat. Mater.* **2012**, *11*, 642−649.
(52) Haugh, M. G.; Vaughan, T. J.; Madl, C. M.; Raftery, R. M.; McNamara, L. M.; O'Brien, F. J.; Heilshorn, S. C. Investigating the Interplay between Substrate Stiffness and Ligand Chemistry in Directing Mesenchymal Stem Cell Differentiation within 3D Macro-Porous Substrates. *Biomaterials* **2018**, *171*, 23−33.
(53) Forte, G.; Pagliari, S.; Ebara, M.; Uto, K.; Van Tam, J. K.; Romanazzo, S.; Escobedo-Lucea, C.; Romano, E.; Di Nardo, P.; Traversa, E.; et al. Substrate Stiffness Modulates Gene Expression and Phenotype in Neonatal Cardiomyocytes *In Vitro*. *Tissue Eng., Part A* **2012**, *18*, 1837−1848.
(54) Mauretti, A.; Bax, N. A. M.; Van Marion, M. H.; Goumans, M. J.; Sahlgren, C.; Bouten, C. V. C. Cardiomyocyte Progenitor Cell Mechanoresponse Unrevealed: Strain Avoidance and Mechanosome Development. *Integr. Biol.* **2016**, *8*, 991−1001.
(55) Beckerle, M. C. Zyxin: Zinc Fingers at Sites of Cell Adhesion. *BioEssays* **1997**, *19*, 949−957.

DOI: 10.1021/acs.biomac.9b00353
Biomacromolecules 2019, 20, 2360−2371

(56) Choi, M. Y.; Kim, J. T.; Lee, W. J.; Lee, Y.; Park, K. M.; Yang, Y. Il; Park, K. D. Engineered Extracellular Microenvironment with a Tunable Mechanical Property for Controlling Cell Behavior and Cardiomyogenic Fate of Cardiac Stem Cells. *Acta Biomater.* **2017**, *50*, 234−248.
(57) Piccolo, S.; Dupont, S.; Cordenonsi, M. The Biology of YAP/TAZ: Hippo Signaling and Beyond. *Physiol. Rev.* **2014**, *94*, 1287−1312.
(58) Mascharak, S.; Benitez, P. L.; Proctor, A. C.; Madl, C. M.; Hu, K. H.; Dewi, R. E.; Butte, M. J.; Heilshorn, S. C. YAP-Dependent Mechanotransduction Is Required for Proliferation and Migration on Native-like Substrate Topography. *Biomaterials* **2017**, *115*, 155−166.
(59) Mosqueira, D.; Pagliari, S.; Uto, K.; Ebara, M.; Romanazzo, S.; Escobedo-Lucea, C.; Nakanishi, J.; Taniguchi, A.; Franzese, O.; Di Nardo, P.; et al. Hippo Pathway Effectors Control Cardiac Progenitor Cell Fate by Acting as Dynamic Sensors of Substrate Mechanics and Nanostructure. *ACS Nano* **2014**, *8*, 2033−2047.
(60) Dupont, S.; Morsut, L.; Aragona, M.; Enzo, E.; Giulitti, S.; Cordenonsi, M.; Zanconato, F.; Le Digabel, J.; Forcato, M.; Bicciato, S.; et al. Role of YAP/TAZ in Mechanotransduction. *Nature* **2011**, *474*, 179−183.

DOI: 10.1021/acs.biomac.9b00353
Biomacromolecules 2019, 20, 2360−2371